Time-resolved Fourier optical diffuse tomography

M. Xu, M. Lax, and R. R. Alfano

Institute for Ultrafast Spectroscopy and Lasers, New York State Center of Advanced Technology for Ultrafast Photonic Materials and Applications, and Department of Physics, The City College and Graduate Center of City University of New York, New York, NY 10031

Time-resolved Fourier optical diffuse tomography is a novel approach for imaging of objects in a highly scattering turbid medium with use of an incident (near) plane wave. The theory of the propagation of spatial Fourier components of the scattered wave field is presented, along with a fast algorithm for three-dimensional reconstruction in a parallel planar geometry. Examples of successful reconstructions of simulated hidden absorptive or scattering objects embedded inside a human-tissue-like semi-infinite turbid medium are provided. © 2001 Optical Society of America

OCIS codes: 170.6960, 290.7050, 290.1350.

1. INTRODUCTION

Research on the use of near-infrared diffusive light for biomedical imaging and diagnosis has advanced over the past decade because of the potential of the technique to be a safe, noninvasive, affordable, and superior diagnostics tool.[1–3] In the search for a methodology that provides fast data acquisition and reconstruction to perform imaging with high resolution in real time, a variety of techniques have been explored including the use of time-resolved picosecond pulses, continuous waves, and diffuse photon-density waves. Most methods reconstruct three-dimensional (3D) optical property maps (OPMs) by matrix inversion, by iterative techniques, or by 3D rendering of two-dimensional (2D) projection images.[4–8] The degree of difficulty of inverting the whole 3D map at one time is usually time prohibitive when the number of volume elements involved increases, and 3D rendering of two-dimensional projection images requires extra depth information of inhomogeneities inside turbid media to behave well, and it has other limitations.[7,9]

In this paper, we first introduce the theory of propagation of the spatial Fourier component of the scattered wave field inside a turbid medium. We then develop a new optical diffuse imaging methodology based on this theory, using the two-dimensional Fourier transform of photon intensity on a plane to detect inhomogeneities in a highly scattering turbid medium when the medium is illuminated by a picosecond (near-) plane-wave pulse. In such a spatial Fourier space, the picture of photon migration is much simplified in the sense that different spatial frequency components of the OPM (2D Fourier transform on the *xy* plane) are decoupled from one another and depend only on the corresponding spatial frequency component of the photon intensity on the detector plane. On the basis of this observation, we obtain a super-fast reconstruction of a 3D OPM by matrix inversion of each spatial component independently. The effect of noise is explicitly handled by controlling the set of spatial frequency components and the regularization parameters used in the matrix inversion. After a rigorous account of the theory and a brief description of the algorithm, examples of reconstruction, by using backscattered photons, of absorptive and scattering inhomogeneities located up to 2 cm below the surface of a human-tissue-like semi-infinite turbid medium are presented.

2. THEORY

The propagation of photon density $\phi(\mathbf{r}, t)$ at position $\mathbf{r}$ and time t in a highly scattering turbid medium can be described by the diffusion equation

$$\frac{\partial}{\partial t}\phi(\mathbf{r}, t) - c\nabla \cdot D(\mathbf{r})\nabla\phi(\mathbf{r}, t) + c\mu_a(\mathbf{r})\phi(\mathbf{r}, t)$$

$$= S(\mathbf{r}, t). \quad (1)$$

The absorption coefficient μ_a (per unit length), and the diffusion coefficient $D = 1/(3\mu_s')$, where μ_s' is the reduced scattering coefficient, may depend on the position in the medium; c is the speed of light inside the medium, and S is the source term describing the density of photons generated per second.

For the case of a uniform medium and an incident source $S(\mathbf{r}, t)$ ($S = 0$ when $t < 0$), the incident wave field is $\phi_i(\mathbf{r}, t) = \int d^3\mathbf{r}' \int_0^t dt' S(\mathbf{r}', t')G(\mathbf{r}, \mathbf{r}', t - t')$ where $G(\mathbf{r}, \mathbf{r}', t)$ is the Green's function for the diffusion equation in a uniform turbid medium. When some weak inhomogeneities (objects such as tumors) are embedded in the medium, we write

$$\mu_{a,\mathrm{obj}}(\mathbf{r}) = \mu_a + \delta\mu_a(\mathbf{r}),$$

$$\mu_{s,\mathrm{obj}}'(\mathbf{r}) = \mu_s' + \delta\mu_s'(\mathbf{r}), \quad (2)$$

where μ_a and μ_s' are the constant absorption and reduced scattering coefficients of the otherwise homogeneous medium and $\mu_{a,\mathrm{obj}}(\mathbf{r})$ and $\mu_{s,\mathrm{obj}}'(\mathbf{r})$ are the absorption and reduced scattering coefficients of the embedded inhomogeneity that are spatially dependent. Plugging Eq. (2) into

Eq. (1) and noting the diffusion parameter of the inhomogeneity $D_{obj}(\mathbf{r}) = D + \delta D(\mathbf{r}) = 1/(3\mu_s') - \delta\mu_s'(\mathbf{r})/(3\mu_s'^2)$, we have

$$\frac{\partial}{\partial t}\phi(\mathbf{r}, t) - Dc\nabla^2\phi(\mathbf{r}, t) + \mu_a c\,\phi(\mathbf{r}, t)$$

$$= S(\mathbf{r}, t) + c\nabla \cdot \delta D(\mathbf{r})\nabla\phi(\mathbf{r}, t) - c\,\delta\mu_a(\mathbf{r})\phi(\mathbf{r}, t). \quad (3)$$

The complete right-hand side of Eq. (3) now acts as the source term, of which $S(\mathbf{r}, t)$ contributes to the unperturbed wave field $\phi_0 = \phi_i(\mathbf{r}, t)$ and the rest of the terms contribute to the scattered wave field,

$$\phi_s(\mathbf{r}, t)$$

$$= \phi(\mathbf{r}, t) - \phi_0(\mathbf{r}, t)$$

$$= \int d^3\mathbf{r}'\int_0^t dt'\, G(\mathbf{r}, \mathbf{r}', t - t')$$

$$\times\, [c\nabla_{\mathbf{r}'} \cdot \delta D(\mathbf{r}')\nabla_{\mathbf{r}'}\phi(\mathbf{r}', t')$$

$$-\, c\,\delta\mu_a(\mathbf{r}')\phi(\mathbf{r}', t')]$$

$$= -\int d^3\mathbf{r}'\int_0^t dt'\, G(\mathbf{r}, \mathbf{r}', t - t')\delta\mu_a(\mathbf{r}')c\,\phi(\mathbf{r}', t')$$

$$+\int d^3\mathbf{r}'\int_0^t dt'\frac{\delta\mu_s'(\mathbf{r}')c}{3\mu_s'^2}\nabla_{\mathbf{r}'}G(\mathbf{r}, \mathbf{r}', t - t')$$

$$\cdot\,\nabla_{\mathbf{r}'}\phi(\mathbf{r}', t'), \quad (4)$$

after integration by parts.

To first order in the variation of optical absorption and reduced scattering coefficients, we can just replace $\phi(\mathbf{r}', t')$ in Eq. (4) with ϕ_i, i.e., the total wave field is a superposition of the incident wave field ϕ_i and the singly scattered wave field ϕ_s. This is the well-known Born approximation.

Now consider the configuration of the frequently studied parallel planar geometry (slab or semi-infinite) with its boundaries at $z = 0$ and $z = d$ ($d = +\infty$ for semi-infinite geometry). The exact Green's function is[10]

$$G(\mathbf{r}, \mathbf{r}', t) = \frac{1}{4\pi Dct}\exp\!\left(-\frac{|\rho - \rho'|^2}{4Dct} - \mu_a ct\right)$$

$$\times\, G_z(z, z', t), \quad (t > 0), \quad (5)$$

where $\rho = (x, y)$, $\rho' = (x', y')$. $G_z(z, z', t)$ is chosen according to the boundary condition of the parallel planar geometry and depends only on time t and the z coordinates of the source position $\mathbf{r}$ and the target position $\mathbf{r}'$. Its two-dimensional Fourier transform on ρ is

$$\hat{G}(\mathbf{q}, z, \rho', z', t) = \int d^2\rho\, G(\rho, z, \rho', z', t)\exp\left(-i\mathbf{q} \cdot \rho\right)$$

$$= \exp(-i\mathbf{q} \cdot \rho' - Dctq^2$$

$$-\,\mu_a ct)G_z(z, z', t)$$

$$= \hat{G}(\mathbf{q}, z, z', t')\exp(-i\mathbf{q} \cdot \rho'). \quad (6)$$

For simplicity, we restrict ourselves first to the case of a pure absorptive perturbation ($\delta\mu_a \neq 0$ and $\delta\mu_s' = 0$)

and of an incident pulse $S(\mathbf{r}, t) = S(\rho)\delta(z - z_s)\delta(t)$. The scattered wave field on a plane $0 < z < d$ is thus

$$\phi_s(\rho, z, t)$$

$$= -\int d^3\mathbf{r}'\int d^2\rho''\int_0^t dt'\, G(\mathbf{r}, \mathbf{r}', t - t')\delta\mu_a(\mathbf{r}')$$

$$\times\, cS(\rho'')G(\mathbf{r}', \rho'', z_s, t') \quad (7)$$

from Eq. (4) after ϕ is replaced by ϕ_i. Inside Eq. (7), expand the source term $S(\rho'')$ and the Green's functions $G(\mathbf{r}, \mathbf{r}', t - t')$ and $G(\mathbf{r}', \rho'', z_s, t')$ into integrals of their Fourier components; thus we find

$$\phi_s(\rho, z, t) = -\frac{1}{(4\pi^2)^3}\int d^2\rho'\int dz'\int d^2\rho''\int_0^t dt'$$

$$\times\int d^2\mathbf{q}\hat{G}(\mathbf{q}, z, z', t - t')$$

$$\times\, \exp[i\mathbf{q} \cdot (\rho - \rho')]$$

$$\times\, \delta\mu_a(\rho', z')c\int d^2\mathbf{q}''\hat{S}(\mathbf{q}'')\exp(i\mathbf{q}'' \cdot \rho'')$$

$$\times\int d^2\mathbf{q}'\hat{G}(\mathbf{q}', z', z_s, t')$$

$$\times\, \exp[i\mathbf{q}' \cdot (\rho' - \rho'')]$$

$$= -\frac{c}{(4\pi^2)^3}\int d^2\mathbf{q}\int d^2\mathbf{q}'\int d^2\mathbf{q}''\int_0^t dt'\int dz'$$

$$\times\, \exp(i\mathbf{q} \cdot \rho)\hat{G}(\mathbf{q}, z, z', t - t')$$

$$\times\, \hat{S}(\mathbf{q}'')\hat{G}(\mathbf{q}', z', z_s, t')$$

$$\times\int d^2\rho'\,\delta\mu_a(\rho', z')\exp[-i\rho'$$

$$\cdot\,(\mathbf{q} - \mathbf{q}')]\int d^2\rho''\exp[i\rho'' \cdot (\mathbf{q}'' - \mathbf{q}')]$$

$$= -\frac{c}{(4\pi^2)^2}\int d^2\mathbf{q}\int d^2\mathbf{q}'\int_0^t dt'\int dz'$$

$$\times\, \exp(i\mathbf{q} \cdot \rho)\hat{G}(\mathbf{q}, z, z', t - t')$$

$$\times\, \delta\hat{\mu}_a(\mathbf{q} - \mathbf{q}', z')\hat{S}(\mathbf{q}')\hat{G}(\mathbf{q}', z', z_s, t'), \quad (8)$$

where

$$\hat{S}(\mathbf{q}) = \hat{S}(\mathbf{q}, z_s) = \int d^2\rho S(\rho, z_s)\exp(-i\mathbf{q} \cdot \rho),$$

$$\delta\hat{\mu}_a(\mathbf{q}, z) = \int d^2\rho\,\delta\mu_a(\rho, z)\exp(-i\mathbf{q} \cdot \rho)$$

are 2D Fourier transforms of the source on the $z = z_s$ plane and of the perturbation of the absorption coefficient over the $z = z$ plane, respectively. Finally, we recognize the 2D Fourier transform of the scattered wave field $\phi_s(\rho, z, t)$ on a plane z for the case of a pure absorptive perturbation:

$$\hat{\phi}(\mathbf{q}, z, t) = -\frac{c}{4\pi^2} \int d^2\mathbf{q}' dz' \delta\hat{\mu}_a(\mathbf{q} - \mathbf{q}', z') \hat{S}(\mathbf{q}', z_s)$$

$$\times \int_0^t dt' \hat{G}(\mathbf{q}, z, z', t - t') \hat{G}(\mathbf{q}', z', z_s, t').$$

$$(9)$$

In a similar fashion, for the case of a pure scattering perturbation ($\delta\mu_a = 0$ and $\delta\mu_s' \neq 0$), the 2D Fourier transform of the scattered wave field is

$$\hat{\phi}_s(\mathbf{q}, z, t)$$

$$= \frac{c}{12\pi^2\mu_s'^2} \int d^2\mathbf{q}' dz' \delta\hat{\mu}_s'(\mathbf{q} - \mathbf{q}', z') \hat{S}(\mathbf{q}', z_s)$$

$$\times \int_0^t dt' \left[\mathbf{q} \cdot \mathbf{q}' \hat{G}(\mathbf{q}, z, z', t - t') \hat{G}(\mathbf{q}', z', z_s, t') \right.$$

$$\left. + \frac{\partial\hat{G}(\mathbf{q}, z, z', t - t')}{\partial z'} \frac{\partial\hat{G}(\mathbf{q}', z', z_s, t')}{\partial z'} \right]. \quad (10)$$

The general Fourier scattered wave field is the sum of Eq. (9) and Eq. (10). Denoting the convolutions

$$w_a(\mathbf{q}, \mathbf{q}', z, t; z') = \int_0^t dt' \hat{G}(\mathbf{q}, z, z', t$$

$$- t') \hat{G}(\mathbf{q}', z', z_s, t'),$$

$$w_s(\mathbf{q}, \mathbf{q}', z, t; z') = \int_0^t dt' \frac{\partial\hat{G}(\mathbf{q}, z, z', t - t')}{\partial z'}$$

$$\times \frac{\partial\hat{G}(\mathbf{q}', z', z_s, t')}{\partial z'}, \quad (11)$$

which are the weight functions involved in the propagation of spatial Fourier components of the scattered wave field, we have

$$\hat{\phi}_s(\mathbf{q}, z, t)$$

$$= -\frac{c}{4\pi^2} \int d^2\mathbf{q}' dz' \delta\hat{\mu}_a(\mathbf{q} - \mathbf{q}', z')$$

$$\times \hat{S}(\mathbf{q}', z_s) w_a(\mathbf{q}, \mathbf{q}', z, t; z') + \frac{c}{12\pi^2\mu_s'^2}$$

$$\times \int d^2\mathbf{q}' dz' \delta\hat{\mu}_s'(\mathbf{q} - \mathbf{q}', z') \hat{S}(\mathbf{q}', z_s)$$

$$\times [\mathbf{q} \cdot \mathbf{q}' w_a(\mathbf{q}, \mathbf{q}', z, t; z') + w_s(\mathbf{q}, \mathbf{q}', z, t; z')].$$

$$(12)$$

For the simple case in which the incident wave is a plane-wave pulse (see Appendix A for justification), i.e., $S(\mathbf{r}, t) = S\delta(z - z_s)\delta(t)$ where S is a constant, such that $\hat{S}(\mathbf{q}, z_s) = 4\pi^2 S\delta(\mathbf{q})$, Eq. (12) simplifies to

$$\hat{\phi}_s(\mathbf{q}, z, t) = -Sc \int dz' \left[\delta\hat{\mu}_a(\mathbf{q}, z') w_a(\mathbf{q}, 0, z, t; z') \right.$$

$$\left. - \frac{\delta\hat{\mu}_s'(\mathbf{q}, z')}{3\mu_s'^2} w_s(\mathbf{q}, 0, z, t; z') \right]. \quad (13)$$

The most salient feature of the above result [Eq. (13)] is that different spatial frequency components of $\delta\hat{\mu}_a$ and $\delta\hat{\mu}_s'$ are decoupled from one another, and the $\mathbf{q}$ component of the optical parameters depends only on the corresponding spatial frequency component of the scattered wave field $\hat{\phi}_s(\mathbf{q}, z, t)$. Thus the dimension of the inverse problem to be solved below is greatly reduced, as is the computation time.

If we approximate the integration over z' by a summation and fix $z = z_d$ at the detection plane (omitting z hereafter), the Fourier scattered wave field on the detection plane is

$$\hat{\phi}_s(\mathbf{q}, t) = Sc\Delta z \sum_{j=1}^{N_z} \left[-\delta\hat{\mu}_a(\mathbf{q}, z_j) w_a(\mathbf{q}, 0, t; z_j) \right.$$

$$\left. + \frac{\delta\hat{\mu}_s'(\mathbf{q}, z_j)}{3\mu_s'^2} w_s(\mathbf{q}, 0, t; z_j) \right], \quad (14)$$

where Δz is the discretized step size, N_z is the total number of slices (layers) in the z direction between the source plane and the detection plane, and z_j is the z coordinate of the central position of layer j.

If we set $\mathbf{q} = 0$ in Eq. (14),

$$\hat{\phi}_s(0, t) = Sc\Delta z \sum_{j=1}^{N_z} \left[-\delta\hat{\mu}_a(0, z_j) w_a(0, 0, t; z_j) \right.$$

$$\left. + \frac{\delta\hat{\mu}_s'(0, z_j)}{3\mu_s'^2} w_s(0, 0, t; z_j) \right], \quad (15)$$

the zero spatial frequency components $\delta\hat{\mu}_a(0, z_j)$ and $\delta\hat{\mu}_s'(0, z_j)$ can be readily solved without the need for a complete reconstruction. Owing to the nature of Fourier transform, they just provide the profile of the amount of total perturbation of absorption and reduced scattering coefficients per slice, i.e., the depth profile of the inhomogeneities.

The whole 3D map of absorption and reduced scattering coefficients is thus constructed through an inverse Fourier transform from all the $\mathbf{q}$ components of $\delta\hat{\mu}_a$ and $\delta\hat{\mu}_s'$ at different depths, each of which is solved independently from a series of time-resolved scattered wave field $\hat{\phi}_s$ by Eq. (14).

A schematic diagram of the procedure of image reconstruction is shown in Fig. 1. The maximum spatial frequency (cutoff frequency) of the components used in the inversion is determined through a signal-to-noise-ratio analysis in which the Fourier components whose magnitudes fall below a threshold (comparable to the noise level) are discarded. The regularization parameter in the matrix inversion is obtained by the robust L-curve method.[11] The L-corner finder, which locates the corner by maximum curvature,[12] is implemented and is used to obtain the regularization parameter. Neither visual es-
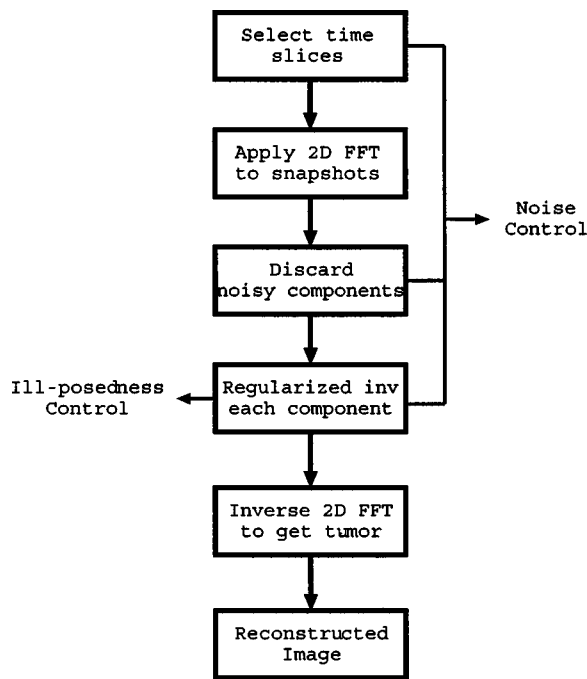
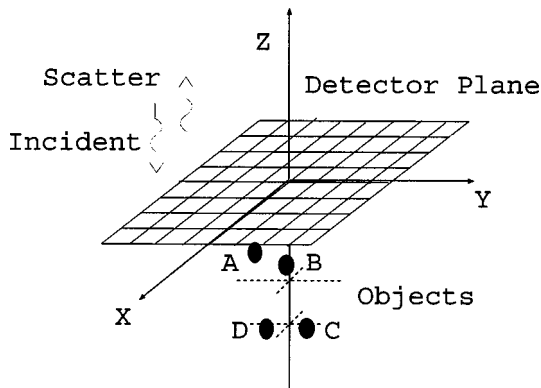Fig. 1.   Schematic diagram of image reconstruction.

Fig. 2.   Geometry for time-resolved Fourier optical diffuse tomography with use of backscattered photons.   The source is a picosecond (near-) plane-wave pulse and a series of snapshots of a $10 \times 10\,\text{cm}^2$ area on the surface are computed as the input to image reconstruction.   Absorptive objects A $(-2.5, -1.875, -0.75)$ cm, B $(-1.25, -0.31, -0.75)$ cm, C $(0.94, 1.56, -1.95)$ cm, and D $(0.94, -0.625, -1.95)$ cm or scattering objects E $(-2.5, -1.875, -0.75)$ cm, F $(-1.25, -0.31, -0.75)$ cm, G $(0.94, 1.56, -1.35)$ cm, and H $(0.94, -0.625, -1.35)$ cm are used in the simulation.

timate nor prior information is required for this procedure.   L curves are different for each spatial frequency $\mathbf{q}$. The regularization parameter is determined from the reconstruction of depth profile (where an inversion for $\mathbf{q} = 0$ is performed).   The same value is then used in the full 3D reconstruction (layer reconstructions, where inversion includes $\mathbf{q} \neq 0$).

Both transmission and backscattering image reconstruction configurations can easily be made by using Eqs. (13) and (14).

3.   SIMULATION

For demonstration purposes, consider a semi-infinite turbid medium ($z < 0$) with its surface at $z = 0$ (Fig. 2), whose absorption coefficient $\mu_a = 0.0033\,\text{mm}^{-1}$ and reduced scattering coefficient $\mu_s' = 1.0\,\text{mm}^{-1}$.

A.   Absorptive Inhomogeneity
Four absorbing objects A, B, C, and D, each $6.25\,\text{mm} \times 6.25\,\text{mm} \times 3\,\text{mm}$ and with absorption coefficient $\mu_{a,\text{obj}} = 0.02\,\text{mm}^{-1}$ and reduced scattering coefficient equal to that of the background, are placed at depth 7.5, 7.5, 19.5, and 19.5 mm below the surface, and their xy coordinates are $(-25, -18.75)$, $(-12.5, -3.1)$, $(9.4, 15.6)$, and $(9.4, 6.25)$ mm, respectively.   The medium is illuminated by an incident pulse of a Gaussian shape of $\exp(-\rho^2/2\sigma^2)$ with $\sigma = 50$ mm inside an aperture of radius 50 mm, propagating along the negative z axis at time $t = 0$.

These parameters are potentially applicable to optical mammography of the compressed-breast-toward-chest setup with use of backscattered photons.   A series of simulated measurements (total $N_t = 15$ snapshots from 300 to 2400 ps) of an area $100\,\text{mm} \times 100\,\text{mm}$ on the surface plane $z = 0$ are generated by using a direct calculation for the Gaussian pulse in $\mathbf{r}$ space.   The simulated data are used as input for inversion after adding a 1%, 5%, or 10% Gaussian noise.

In the reconstruction part, the near-surface region of the turbid medium of depth up to 3 cm is sliced into $N_z = 10$ layers, i.e., $\Delta z = 0.3$ cm, and objects A and B are then located on layer 3, and C and D are located on layer 7.   The detection plane of an area of $10 \times 10\,\text{cm}^2$ is divided uniformly into a $N_x N_y = 32 \times 32$ grid.   Objects A, B, C, and D all take 2×2 elements by this grid.   The results of reconstruction are shown below.
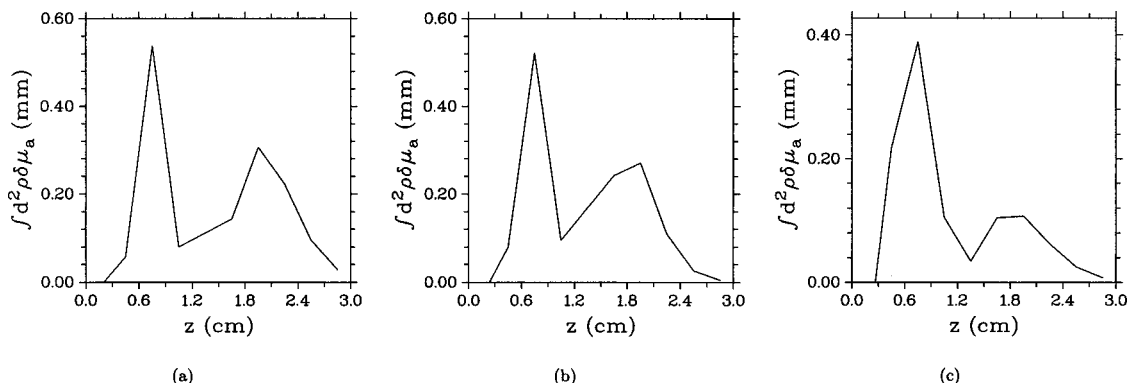

Fig. 3.   Absorption depth profile for (a) with 1% noise, (b) 5% noise, and (c) 10% noise.

1. Depth Profile

The absorption depth profile, i.e., the total absorption perturbation per layer $\int d^2\rho\, \delta\mu_a(\rho, z)$ versus depth z is shown in Fig. 3 with different noise levels for cases (a) 1% noise, (b) 5% noise, and (c) 10% noise. In Fig. 3(a) there is one peak at depth $z = 0.75$ cm (layer 3) where objects A and B are embedded, and another peak at $z = 1.95$ cm (layer 7) where objects C and D are embedded. The width of the first peak at half-height is 0.34 cm, approximately the thickness of one layer (0.3 cm), which means that the depth of objects A and B is resolved very well. The second peak of objects C and D spans two and a half layers with its width of peak at half-height 0.74 cm, but its peak position is still correct.

When the level of noise increases, the peak values of both peaks decrease, and the half-widths increase. The effect on the second peak at $z = 1.95$ cm is much more significant than that on the first one at $z = 0.75$ cm.

2. Layer Reconstruction

The full 3D OPM is reconstructed. The reconstructed absorption coefficients of the layers at the two peak positions are shown in Figs. 4–6 for the three noise levels.

Figure 4 shows that objects A and B are clearly resolved as two objects centered at their original positions with negligible expansion; and objects C and D at depth $z = 1.95$ cm are also detected at the correct central positions, but the resolved images are expanded on the xy plane. With an increase in noise level, the shape of objects A and B blurs from Figs. 4(a) to 5(a) and 6(a), and the blur is even worse for objects C and D under the same condition [from Figs. 4(b) to 5(b) and 6(b)].

At noise level of 1%, the reconstructed absorption parameter for objects A and B is 0.0071 mm^{-1} approximately 36% of the original value 0.02 mm^{-1} of the absorptive inhomogeneity. In other words, the object appears larger in space with a weakened absorption parameter. As the noise level increases, the effect is accentuated with a further reduction in the resolved absorption parameter.

B. Scattering Inhomogeneity

For another example, four scattering objects E, F, G, and H, each 6.25 mm × 6.25 mm × 3 mm and with reduced scattering coefficient $\mu'_{s,\mathrm{obj}} = 0.5$ mm^{-1} and absorption coefficient equal to that of the background, are placed at depth 7.5, 7.5, 13.5, and 13.5 mm below the surface, and

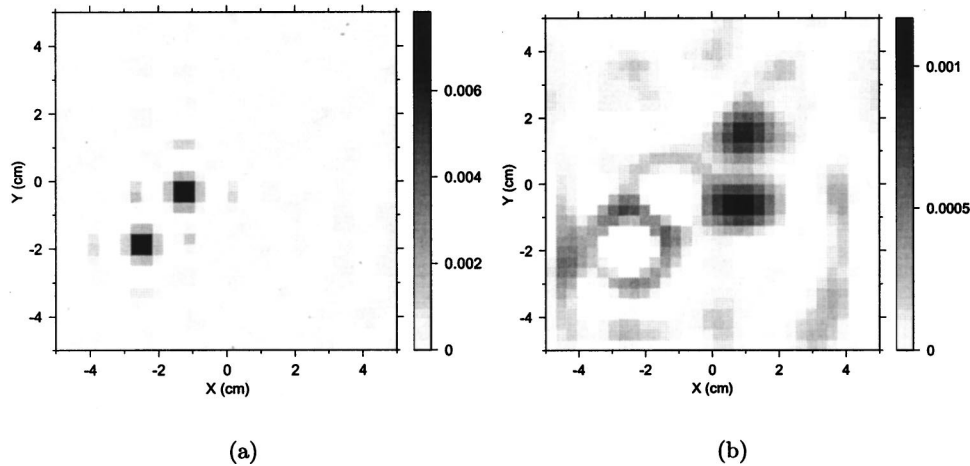(a)   (b)

Fig. 4. Layer reconstruction at a noise level of 1%: (a) resolved objects A (left) and B (right) at $z = 0.75$ cm (layer 3); (b) resolved objects C (upper) and D (lower) at $z = 1.95$ cm (layer 7). The darkness of the pixel represents the resolved absorption coefficient in units of inverse millimeters.
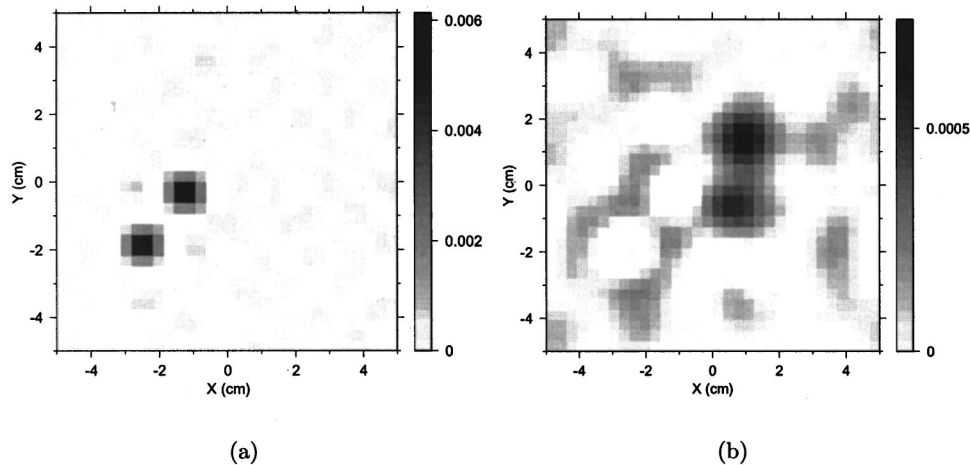

(a)   (b)

Fig. 5. Layer reconstruction at a noise level of 5%: (a) resolved objects A (left) and B (right) at $z = 0.75$ cm (layer 3); (b) resolved objects C (upper) and D (lower) at $z = 1.95$ cm (layer 7). The darkness of the pixel represents the resolved absorption coefficient in units of inverse millimeters.

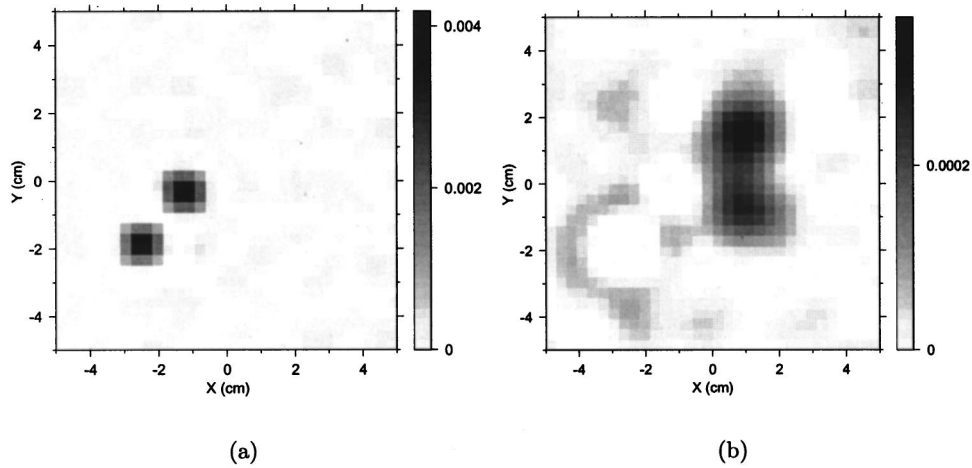(a)   (b)

Fig. 6.   Layer reconstruction at a noise level of 10%:   (a) resolved objects A (left) and B (right) at $z = 0.75$ cm (layer 3); (b) resolved objects C (upper) and D (lower) at $z = 1.95$ cm (layer 7).   The darkness of the pixel represents the resolved absorption coefficient in units of inverse millimeters.
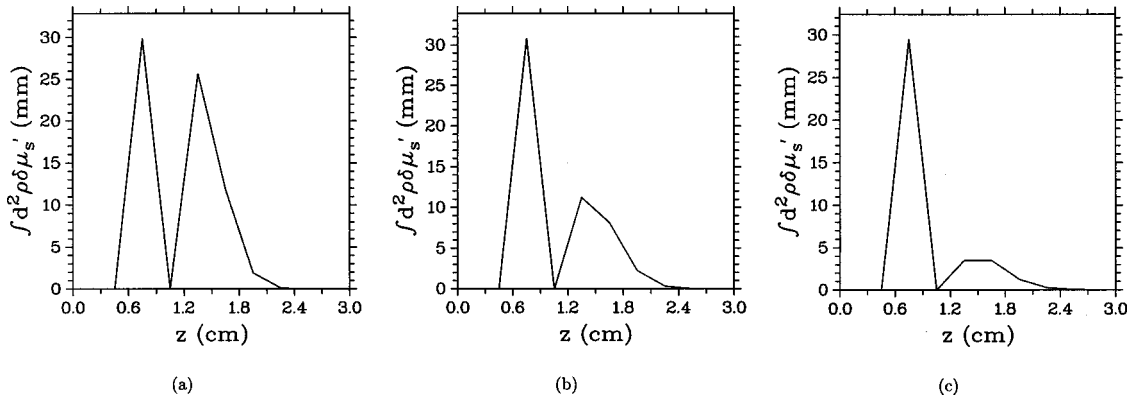

(a)   (b)   (c)

Fig. 7.   Scattering depth profiles for (a) with 1% noise, (b) 5% noise, and (c) 10% noise.

(a)   (b)
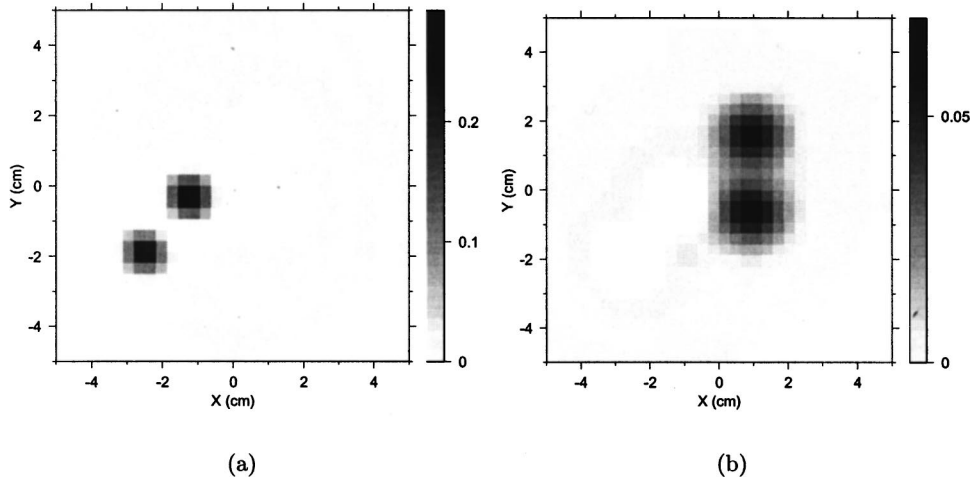
Fig. 8.   Layer reconstruction at a noise level of 1%:   (a) resolved objects E (left) and F (right) at $z = 0.75$ cm (layer 3); (b) resolved objects G (upper) and H (lower) at $z = 1.35$ cm (layer 5).   The darkness of the pixel represents the resolved reduced scattering coefficient in units of inverse millimeters.

their xy coordinates are $(-25, -18.75)$, $(-12.5, -3.1)$, $(9.4, 15.6)$, and $(9.4, 6.25)$ mm, respectively.   Objects E and F are now located on layer 3, and G and H are located on layer 5.   The same source and inversion procedure used in the previous example are used here.   The results of reconstruction are shown below.

1.   Depth Profile
The scattering depth profile is shown in Fig. 7 with different noise levels for cases (a) 1% noise, (b) 5% noise, and (c) 10% noise.   Two peaks are correctly revealed with the first at depth $z = 0.75$ cm (layer 3) and another at $z = 1.35$ cm (layer 5), where objects E and F, G and H are

embedded, respectively. In Fig. 7(a), the width of the first peak at half-height is 0.3 cm and that of the second peak is 0.42 cm. This means that the depth of these objects is resolved quite well.

With an increase in noise level, we observe the same behavior of decreasing quality of depth resolution as in the absorptive case.

2. Layer Reconstruction
The reconstructed scattering coefficients of the layers at the two peak positions (layer 3 and layer 5) are shown in Figs. 8–10 for the three noise levels.

We observe a result similar to that for the absorptive case. Objects E and F are better resolved than objects G and H, which are deeper into the turbid medium, and the noise has a more adverse effect on objects G and H than on objects E and F. The reconstructed reduced scattering coefficient of objects E and F is 0.27 mm^{-1}, approximately 54% of the original value of the embedded scattering inhomogeneity, at a noise level of 1%.

4. DISCUSSION
A fast time-resolved Fourier optical diffuse tomography based on decoupled propagation of spatial Fourier components of the scattered wave field when the medium is illuminated by a plane wave is presented. For a wave not strictly plane but whose zero-frequency component dominates, this approximation is still valid as long as the radial dimensions of the volume where inhomogeneities exist are much smaller than the effective width of the Gaussian beam (see Appendix A).

The image-reconstruction method provided is efficient. The optical parameters at $N_x N_y N_z$ different voxels are reconstructed from a set of N_t measurements by N_k^2 times of inversions of $N_z \times N_z$ matrices, where $N_k^2 < N_x N_y$ is the total number of Fourier components with the noisy ones discarded. Our procedure is much more efficient than a direct reconstruction, where an inversion of $N_x N_y N_z \times N_x N_y N_z$ matrix is involved. The speedup is approximately $O(N_x N_y)$ times faster. The time this algorithm takes to perform a complete 3D reconstruction in the
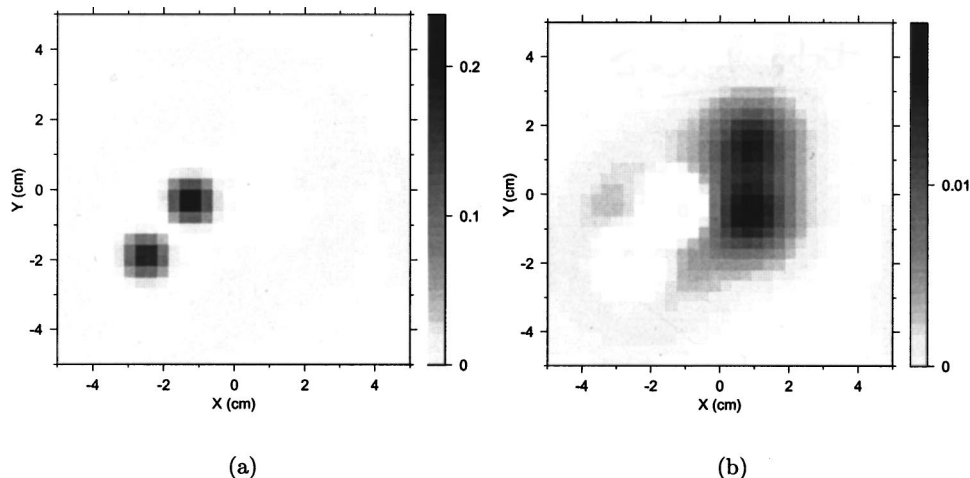

(a)   (b)

Fig. 9. Layer reconstruction at a noise level of 5%: (a) resolved objects E (left) and F (right) at $z = 0.75$ cm (layer 3); (b) resolved objects G (upper) and H (lower) at $z = 1.35$ cm (layer 5). The darkness of the pixel represents the resolved reduced scattering coefficient in units of inverse millimeters.

(a)   (b)
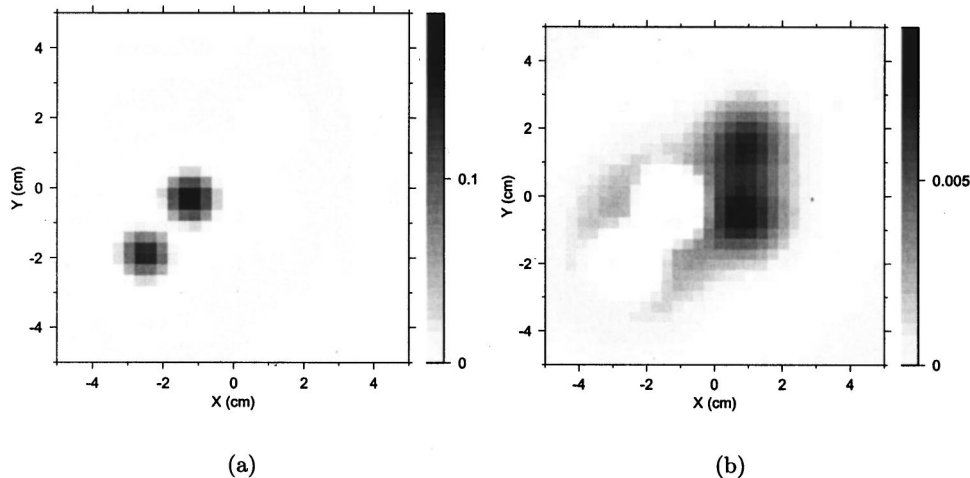
Fig. 10. Layer reconstruction at a noise level of 10%: (a) resolved objects E (left) and F (right) at $z = 0.75$ cm (layer 3); (b) resolved objects G (upper) and H (lower) at $z = 1.35$ cm (layer 5). The darkness of the pixel represents the resolved reduced scattering coefficient in units of inverse millimeters.

above examples (of $32 \times 32 \times 10$ volume elements) is less than half a minute with use of the scripting language Python on one 180-Mhz CPU of an Origin 200 computer from Silicon Graphic Inc. This algorithm scales only linearly with the number of elements in the xy grid, so it can be used to handle much larger data sets in real time with little difficulty.

This approach does not limit the number or the thickness of the inhomogeneities. It allows multiple inhomogeneities, and one inhomogeneity may span several layers.

With little effort, a depth profile (the sum of the perturbation of the optical parameter versus depth) of the inhomogeneities inside a highly scattering turbid medium can be obtained. This information itself may be very useful in some cases. When the inhomogeneity is found to exist only in one layer from the depth profile, the summation in Eq. (14) no longer exists. A direct inverse Fourier transform can thus be used to resolve the inhomogeneity when it is a solely absorptive or scattering perturbation.

APPENDIX A

Equation (12) is the exact formula for calculating the scattered wave field. For a pulse $S(\mathbf{r}, t) = S(\rho) \delta(z - z_s)\delta(t)$ with Gaussian shape $S(\rho) = S_0 \exp(-\rho^2/2\sigma^2)$, we have $\hat{S}(\mathbf{q}) = 2\pi\sigma^2 S_0 \times \exp(-\sigma^2 q^2/2)$ and the first term of Eq. (12),

$$
\begin{aligned}
A &= -\frac{\sigma^2 S_0 c}{2\pi} \int d^2\mathbf{q}' dz' \, \delta\hat{\mu}_a(\mathbf{q} - \mathbf{q}', z') \\
&\quad \times \exp(-\sigma^2 q'^2/2) w_a(\mathbf{q}, \mathbf{q}', z, t; z') \\
&= -\frac{\sigma^2 S_0 c}{2\pi} \int d^2\mathbf{q}' dz' d^2\rho' \, \delta\mu_a(\rho', z') \\
&\quad \times \exp[-i(\mathbf{q} - \mathbf{q}') \cdot \rho' - \sigma^2 q'^2/2] \\
&\quad \times w_a(\mathbf{q}, \mathbf{q}', z, t; z') \\
&= -\frac{\sigma^2 S_0 c}{2\pi} \int d^2\rho' dz' \, \delta\mu_a(\rho', z') \exp(-i\mathbf{q} \cdot \rho') \\
&\quad \times \int_0^t dt' \hat{G}(\mathbf{q}, z, z', t - t') \\
&\quad \times G_z(z', z_s, t') \exp(-\mu_a c t') \\
&\quad \times \int d^2\mathbf{q}' \exp(-\sigma^2 q'^2/2 - Dct' + i\mathbf{q}' \cdot \rho')
\end{aligned}
$$

(16)

after plugging in Eq. (11) and Eq. (6).

The last integral of Eq. (16) can be performed exactly and turns out to be $\pi R^{-2} \exp(-4\rho'^2/R^2)$, where the effec-

tive width $R^2 = \sigma^2/2 + Dct' > \sigma^2/2$. When the inhomogeneities exist inside a region of radial dimension L around the origin of the xy coordinate system that satisfies $L \ll R$, we can approximate $\exp(-4\rho'^2/R^2)$ by 1, which is equivalent to letting $\mathbf{q}' \to 0$, the case of an incident plane wave. The error made by such an approximation is of second order in L/R.

The same analysis can be applied to the second term of Eq. (12).

ACKNOWLEDGMENTS

Corresponding author Min Xu can be reached by e-mail at minxu@sci.ccny.cuny.edu.

REFERENCES

1. B. Chance and R. R. Alfano, eds., *Optical Tomography, Photon Migration, and Spectroscopy of Tissue and Model Media: Theory, Human Studies, and Instrumentation*, Proc. SPIE **2389** (1995).
2. R. R. Alfano, S. G. Demos, and S. K. Gayen, "Advances in optical imaging of biomedical media," Ann. N.Y. Acad. Sci. **820**, 248–271 (1997).
3. J. C. Hebden, S. R. Arridge, and D. T. Delpy, "Optical imaging in medicine: I. Experimental techniques," Phys. Med. Biol. **42**, 825–840 (1997).
4. S. R. Arridge and J. C. Hebden, "Optical imaging in medicine: II. Modelling and reconstruction," Phys. Med. Biol. **42**, 841–853 (1997).
5. W. Cai, B. B. Das, F. Liu, M. Zevallos, M. Lax, and R. R. Alfano, "Time-resolved optical diffusion tomographic image reconstruction in highly scattering turbid media," Proc. Natl. Acad. Sci. U.S.A. **93**, 13561–13564 (1996).
6. X. D. Li, T. Durduran, and A. G. Yodh, "Diffraction tomography for biomedical imaging with diffuse-photon density waves," Opt. Lett. **22**, 573–575 (1997).
7. X. Cheng and D. A. Boas, "Diffuse optical reflection tomography with continuous-wave illumination," Opt. Express **4**, 118–123 (1998), http://www.opticsexpress.org.
8. W. Cai, S. K. Gayen, M. Xu, M. Zevallos, M. Alrubaiee, M. Lax, and R. R. Alfano, "Optical tomographic image reconstruction from ultrafast time-sliced transmission measurements," Appl. Opt. **38**, 1–10 (1999).
9. T. Durduran, J. P. Culver, M. J. Holboke, X. D. Li, and L. Zubkov, "Algorithms for 3D localization and imaging using near-field diffraction tomography with diffuse light," Opt. Express **4**, 247–262 (1999), http://www.opticsexpress.org.
10. S. R. Arridge, "Photon-measurement density functions. Part I. Analytic forms," Appl. Opt. **34**, 7395–7409 (1995).
11. P. C. Hansen, "Analysis of discrete ill-posed problems by means of the L-curve," SIAM Rev. **34**, 561–580 (1992).
12. P. C. Hansen and D. P. O'Leary, "The use of the L-curve in the regularization of discrete ill-posed problems," SIAM J. Sci. Comput. **14**, 1487–1053 (1993).